

Adaptive Passivity-Based Pose Tracking Control of Cable-Driven Parallel Robots for Multiple Attitude Parameterizations

Sze Kwan Cheah, *Student Member, IEEE*, Alex Hayes, *Student Member, IEEE*,
and Ryan J. Caverly, *Member, IEEE*

Abstract—This paper presents a pose tracking controller for a six degree-of-freedom over-constrained cable-driven robot (CDPR). The proposed control method uses an adaptive feedforward-based controller to establish a passive input-output mapping for the CDPR that is used alongside a linear time-invariant strictly positive real feedback controller to guarantee robust closed-loop input-output stability and asymptotic pose trajectory tracking via the passivity theorem. A novelty of the proposed controller is its formulation for use with a range of payload attitude parameterizations, including any unconstrained attitude parameterization, the quaternion, or the direction cosine matrix (DCM). The performance and robustness of the proposed controller is demonstrated through numerical simulations of a CDPR with rigid and flexible cables. The results demonstrate the importance of carefully defining the CDPR's pose error, which is performed in multiplicative fashion when using the quaternion and DCM, and in a specific additive fashion when using unconstrained attitude parameters (e.g., an Euler-angle sequence).

I. INTRODUCTION

Over-constrained cable-driven parallel robots (CDPRs) are a class of parallel robots that make use of a redundant set of tensile cable forces to actuate an end-effector or payload. CDPRs typically feature large workspaces and are capable of relatively high payload accelerations due to their low inertia compared to traditional parallel and serial robotic manipulators. Accurate and robust pose (position and attitude/orientation) control of the CDPR's payload or end-effector is challenging, as over-constrained CDPRs are redundantly actuated, which requires a force distribution algorithm (see [1] for a summary of commonly used methods), and they can have highly uncertain dynamics (e.g., payload with uncertain inertia or flexible/sagging cables). Uncertainty in the CDPR's dynamics can be accounted for with adaptive control techniques, which are often coupled to a specific form of a feedback controller (e.g., a constant-gain proportional-derivative controller) and a specific representation of the payload's attitude (e.g., an Euler-angle sequence) [2]–[6].

Passivity-based control is capable of providing guarantees of robust closed-loop input-output stability for large ranges of system uncertainty and has been widely implemented on serial robotic manipulators for trajectory tracking [7], [8]. Passivity-based control has recently been extended to the robust control of parallel robots [9]–[11], and in particular,

CDPRs [12]–[17]. For example, a robust adaptive passivity-based control method for single degree-of-freedom (DOF) CDPRs capable of tracking desired payload trajectories in the presence of model uncertainty and flexible cables was presented in [15]. Early work on the passivity-based control of CDPRs focused on suspended CDPRs with the same number of cables as payload DOFs [12] or relied on having twice as many cables as payload DOFs in the overconstrained case [13]–[15]. The work of [11], [16], [17] demonstrated that passivity-based task-space translational [11], [16] and pose [17] control of CDPRs can be decoupled from the choice of control allocation method, which greatly expanded its applicability to realistic CDPR configurations that typically feature one or two more cables than payload DOFs.

Virtually all CDPR pose regulation and tracking controllers in the literature make use of Euler angles to compute the attitude portion of the control law (see examples in [2]–[6], [12], [18]–[23]), with the exception of the direction cosine matrix (DCM)-based controller in [17] and the rotation vector-based controller in [24]. In other words, the attitude of the CDPR payload at a given instance in time is computed in terms of an Euler-angle sequence and subtracted from a set of desired Euler angles to form an error signal that is regulated to zero. Although these Euler-angle-based controllers clearly work in practice, it is unnecessary to restrict CDPR pose control to this one choice of attitude parameterization, especially when the rotation matrix or DCM describing the attitude of the CDPR payload is typically available through the forward kinematics needed to operate the CDPR. In addition, advances in nonlinear pose estimation has led to methods that directly estimate the rotation matrix/DCM [25] or quaternion [26] associated with a CDPR payload, making these quantities readily available for control.

This paper presents an adaptive passivity-based CDPR pose tracking controller that uses the passivity theorem to guarantee closed-loop input-output stability and asymptotic tracking of a desired payload pose trajectory, where various attitude parameterizations of the payload attitude can be used. The proposed controller takes inspiration from multiple sources, including passivity-based adaptive controllers designed for CDPRs [6], redundantly-actuated flexible manipulators [27], and spacecraft [28]. The novel contributions of the proposed controller compared to other adaptive CDPR controllers in the literature, including [2]–[6], is 1) its ability to make use of any unconstrained attitude parameterization, the quaternion, or the DCM when computing the pose tracking error and 2) its ease of use with any input-strictly passive

SK. Cheah, A. Hayes, and R. J. Caverly are with the Department of Aerospace Engineering and Mechanics, University of Minnesota, Minneapolis, MN, 55455 USA e-mails: cheah013@umn.edu, hayes455@umn.edu, rcaverly@umn.edu.

(ISP) or strictly positive real (SPR) feedback controller. The first contribution has the potential to lead to a more homogeneous CDPR operation framework, where the same attitude parameterization can be used both for kinematics and motion control. At a minimum, the proposed control method provides the CDPR operator with a choice as to which attitude parameterization they desire to use for feedback, which, to the best of the knowledge of the authors, is a limitation in the CDPR literature, where Euler-angle sequences are almost exclusively used for control (exceptions include a DCM-based pose-regulation controller was used in [17] and a rotation-vector-based controller was implemented in [24]). The second contribution related to the use of an ISP or SPR controller has practical benefits, as the design of the feedback controller can be decoupled from the closed-loop stability analysis and practical control designs, such as a low-pass control gain can be implemented.

The form of the proposed passivity-based adaptive controller stems from [7], [29] and makes use of advances in [27], [28], where attitude parameterizations were incorporated within passivity-based control. The novelty of the proposed controller compared to the theory developed in [27] for flexible manipulators, includes extending its use to the quaternion or DCM, as well as its application and validation on a CDPR. The quaternion-based spacecraft attitude controller in [28] is extended to CDPR pose tracking to yield the proposed quaternion-based method. The work in this paper is also an extension of the preliminary study on passivity-based pose regulation of a CDPR in [17], which assumed knowledge of the CDPR dynamics, did not provide any mathematical guarantees of pose tracking error convergence, and was limited to the use of the DCM to represent the attitude of the CDPR's payload. The control method proposed in this paper removes these restrictions and assumptions.

The remainder of this paper proceeds as follows. Important preliminaries, including notation, theorems, and a description of the CDPR kinematics and dynamics are presented in Section II. Section III presents the proposed adaptive passivity-based control formulation using unconstrained attitude parameterizations, the quaternion, and the DCM. Numerical simulation results are included in Section IV, followed by concluding remarks in Section V.

II. PRELIMINARIES

Notation and theorems used throughout the paper are presented in this section, followed by an overview of the CDPR kinematics and dynamics considered in this work.

A. Notation, Definitions and Theorems

For this paper, the identity matrix and a matrix of zeros are respectively written as $\mathbf{1}$ and $\mathbf{0}$. Matrices are represented in bold (e.g., $\mathbf{A} \in \mathbb{R}^{n \times m}$). Positive definite matrices are represented by $\mathbf{A} = \mathbf{A}^\top > 0$. The cross operator, $(\cdot)^\times$:

$\mathbb{R}^3 \rightarrow \mathfrak{so}(3)$, is defined as

$$\mathbf{v}^\times = \begin{bmatrix} 0 & -v_3 & v_2 \\ v_3 & 0 & -v_1 \\ -v_2 & v_1 & 0 \end{bmatrix},$$

where $\mathbf{v}^\top = [v_1 \ v_2 \ v_3]$ and $\mathfrak{so}(3) = \{\mathbf{S} \in \mathbb{R}^{3 \times 3} | \mathbf{S} + \mathbf{S}^\top = \mathbf{0}\}$. The reverse or uncross operator, $(\cdot)^\vee : \mathbb{R}^{3 \times 3} \rightarrow \mathbb{R}^3$, is defined as $\mathbf{A}^\vee = [a_1 \ a_2 \ a_3]^\top$, where $\mathbf{A} = -\mathbf{A}^\top = (\mathbf{A}^\vee)^\times$. The antisymmetric projection operator, $\mathcal{P}(\cdot) : \mathbb{R}^{3 \times 3} \rightarrow \mathfrak{so}(3)$, projects a matrix $\mathbf{U} \in \mathbb{R}^{3 \times 3}$ to the set of antisymmetric matrices, where $\mathcal{P}(\mathbf{U}) = \frac{1}{2}(\mathbf{U} - \mathbf{U}^\top)$. For $\mathbf{v} \in \mathbb{R}^3$ and $\mathbf{U} \in \mathbb{R}^{3 \times 3}$, it follows that [30]

$$\frac{1}{2} \text{tr}(\mathbf{v}^\times \mathbf{U}) = -\mathbf{v}^\top \mathcal{P}(\mathbf{U})^\vee. \quad (1)$$

Another useful cross operator identity is given by [31]

$$\mathbf{v}^\times \mathbf{A} + \mathbf{A}^\top \mathbf{v}^\times = ((\text{tr}(\mathbf{A})\mathbf{1} - \mathbf{A})\mathbf{v})^\times, \quad (2)$$

where $\mathbf{v} \in \mathbb{R}^3$ and $\mathbf{A} \in \mathbb{R}^{3 \times 3}$. The signal $\mathbf{y}(t)$ satisfies $\mathbf{y} \in \mathcal{L}_2$ if $\|\mathbf{y}\|_2^2 = \int_0^\infty \mathbf{y}^\top(t)\mathbf{y}(t)dt < \infty$. The signal $\mathbf{y}(t)$ satisfies $\mathbf{y} \in \mathcal{L}_{2e}$ if $\mathbf{y}_T \in \mathcal{L}_2$ for all $T \in \mathbb{R}_{\geq 0}$, where $\mathbf{y}_T(t) = \mathbf{y}(t)$ for $0 \leq t \leq T$ and $\mathbf{y}_T(t) = \mathbf{0}$ for $T < t$.

The attitude of reference frame \mathcal{F}_p relative to reference frame \mathcal{F}_a is described by the DCM \mathbf{C}_{pa} , which is a member of the special orthogonal group $SO(3)$, where $SO(3) = \{\mathbf{C} \in \mathbb{R}^{3 \times 3} | \mathbf{C}^\top \mathbf{C} = \mathbf{1}, \det(\mathbf{C}) = 1\}$. The DCM \mathbf{C}_{pa} is related to the rotation matrix, \mathbf{R} that rotates frame \mathcal{F}_a to \mathcal{F}_p by $\mathbf{C}_{pa} = \mathbf{R}^\top$. Parameterizations of the DCM are represented in this paper as $\mathbf{q}^{pa} \in \mathbb{R}^n$, examples of which include an Euler-angle sequence ($\mathbf{q}^{pa} \in \mathbb{R}^3$), the quaternion ($\mathbf{q}^{pa} \in \mathbb{R}^4$), or even the columns of the DCM ($\mathbf{q}^{pa} \in \mathbb{R}^9$). Poisson's equation relates the angular velocity to the time derivative of the DCM as $\dot{\mathbf{C}}_{pa} = -\boldsymbol{\omega}^{pa \times} \mathbf{C}_{pa}$, where $\boldsymbol{\omega}^{pa}$ is the angular velocity of \mathcal{F}_p relative to \mathcal{F}_a resolved in \mathcal{F}_p . The attitude parameterization rates are related to angular velocity by $\boldsymbol{\omega}^{pa} = \mathbf{S}(\mathbf{q}^{pa})\dot{\mathbf{q}}^{pa}$, where $\mathbf{S}(\mathbf{q}^{pa})$ is a mapping matrix whose contents depends on the choice of attitude parameterization [32], [33].

Definition 1 (Passivity [8]): The input-output mapping $\mathbf{u} \mapsto \mathbf{y}$ associated with the operator $\mathcal{G} : \mathcal{L}_{2e} \rightarrow \mathcal{L}_{2e}$, where $\mathbf{y} = \mathcal{G}(\mathbf{u})$, is ISP if for all $\mathbf{u} \in \mathcal{L}_{2e}$ and $T \in \mathbb{R}_{\geq 0}$ there exist $\delta \in \mathbb{R}_{>0}$ and $\beta \in \mathbb{R}$ such that

$$\int_0^T \mathbf{y}^\top(t)\mathbf{u}(t)dt \geq \delta \|\mathbf{u}_T\|_2^2 + \beta. \quad (3)$$

If (3) is satisfied with $\delta = 0$, then $\mathbf{u} \mapsto \mathbf{y}$ is passive. The scalar β is a constant related to initial conditions.

B. CDPR Kinematics and Dynamics

Consider an over-constrained CDPR with m rigid cables actuated by winches and connected to a rigid-body payload, where $m > 6$, as shown in Fig. 1. The CDPR's equations of motion in task space are given as [34]

$$\mathbf{M}(\boldsymbol{\rho})\dot{\boldsymbol{\nu}} + \mathbf{D}(\boldsymbol{\rho}, \boldsymbol{\nu})\boldsymbol{\nu} + \mathbf{g}(\boldsymbol{\rho}) = \mathbf{\Pi}^\top(\boldsymbol{\rho})\boldsymbol{\tau}, \quad (4)$$

where $\boldsymbol{\rho}^\top = [\mathbf{r}^\top \ \mathbf{q}^{pa \top}]$ represents the payload's pose, $\mathbf{r} \in \mathbb{R}^3$ is the position of the payload's center of mass relative

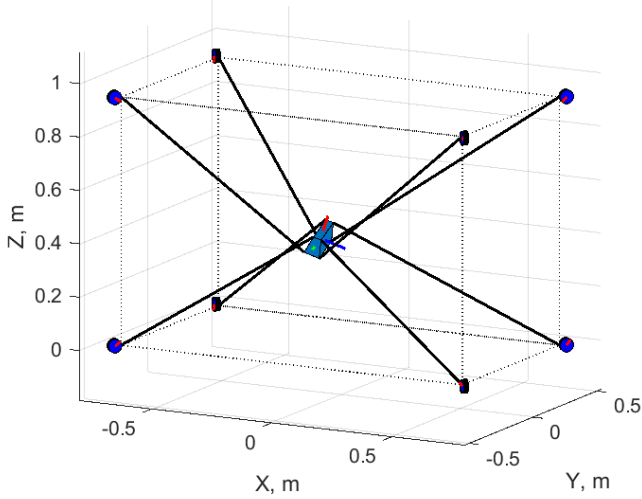


Fig. 1. A 6 DOF CDRP with 8 flexible cables and a rigid-body payload.

to a point at the origin of an inertial frame \mathcal{F}_a resolved in \mathcal{F}_a , and $\mathbf{q}^{pa} \in \mathbb{R}^n$ is an attitude parameterization of the payload-fixed reference frame \mathcal{F}_p relative to \mathcal{F}_a . The augmented payload velocity is given by $\boldsymbol{\nu}^\top = [\dot{\mathbf{r}}^\top \ \boldsymbol{\omega}^{pa\top}]$, where $\boldsymbol{\omega}^{pa} \in \mathbb{R}^3$ is the angular velocity of \mathcal{F}_p relative to \mathcal{F}_a resolved in \mathcal{F}_p . The torques applied by the winches are denoted as $\boldsymbol{\tau}^\top = [\tau_1 \ \dots \ \tau_m]$. The remaining terms in (4) are the mass matrix $\mathbf{M}(\boldsymbol{\rho}) = \mathbf{M}^\top(\boldsymbol{\rho}) > 0$, the nonlinear term $\mathbf{D}(\boldsymbol{\rho}, \boldsymbol{\nu})$, which contains centrifugal and Coriolis forces, and the gravitational term $\mathbf{g}(\boldsymbol{\rho})$. Furthermore, it is known that $\dot{\mathbf{M}}(\boldsymbol{\rho}) - 2\mathbf{D}(\boldsymbol{\rho}, \boldsymbol{\nu})$ is skew-symmetric [34]. The winch torques are distributed through the wrench matrix $\boldsymbol{\Pi}(\boldsymbol{\rho}) \in \mathbb{R}^{m \times 6}$, which is uniquely defined through inverse velocity kinematics and is full rank when the payload remains within its wrench-feasible workspace.

III. CONTROL FORMULATION AND PASSIVITY & STABILITY ANALYSES

The pose tracking controller is presented in this section, where the objective is to ensure $\mathbf{r} \rightarrow \mathbf{r}_d$ and $\mathbf{q}^{pa} \rightarrow \mathbf{q}^{da}$ as $t \rightarrow \infty$, where \mathbf{r}_d and \mathbf{q}^{da} describe the desired position and attitude trajectories of the CDRP payload, respectively. As with previous preliminary work on the passivity-based control of CDRPs [17], the controller is formulated in terms of

$$\mathbf{f} = \boldsymbol{\Pi}^\top(\boldsymbol{\rho})\boldsymbol{\tau},$$

where $\mathbf{f} \in \mathbb{R}^6$ is the control wrench to be applied to the payload (i.e., its first three elements are a force resolved in \mathcal{F}_a and its last three elements are a torque resolved in \mathcal{F}_p). See [1] for a summary of a force distribution methods that can be used to determine the torques $\boldsymbol{\tau}$ that generate the desired control wrench. Force distribution is not a contribution of this work and the following analysis and results are valid for any method, provided $\mathbf{f} = \boldsymbol{\Pi}^\top(\boldsymbol{\rho})\boldsymbol{\tau}$.

The proposed control input is described by

$$\mathbf{f} = \mathbf{f}_{ff} + \mathbf{f}_{fb}, \quad (5)$$

where \mathbf{f}_{ff} is an adaptive feedforward-based input and \mathbf{f}_{fb} is a feedback input. The remainder of this section outlines the proposed adaptive feedforward-based and feedback control inputs, formulations of the pose tracking errors for different attitude parameterizations, along with proofs of passivity and closed-loop trajectory tracking convergence.

A. Adaptive Feedforward-Based Control

The adaptive feedforward-based control input is derived by first considering a desired feedforward-based input

$$\mathbf{f}_d = \begin{bmatrix} m_p \mathbf{1} & \mathbf{0} \\ \mathbf{0} & \mathbf{I}_p \end{bmatrix} \dot{\boldsymbol{\nu}}_r + \begin{bmatrix} \mathbf{0} & \mathbf{0} \\ \mathbf{0} & \boldsymbol{\omega}^{pa \times} \mathbf{I}_p \end{bmatrix} \boldsymbol{\nu}_r + \begin{bmatrix} m_p g \mathbf{1}_3 \\ \mathbf{0} \end{bmatrix} \quad (6)$$

where $m_p \in \mathbb{R}$ and $\mathbf{I}_p = \mathbf{I}_p^\top \in \mathbb{R}^{3 \times 3}$ represent the constant mass and inertia of the payload, and $\mathbf{1}_3 = [0 \ 0 \ 1]^\top$. Note that (6) is equivalent to (4), with the assumption that the dynamics of the CDRP are dominated by those of its rigid-body payload and the replacement of $\boldsymbol{\nu}$ by $\boldsymbol{\nu}_r$, which represents the virtual filtered rate trajectory defined as [27]

$$\boldsymbol{\nu}_r = \boldsymbol{\nu}_d - \mathbf{P}\boldsymbol{\Lambda}\tilde{\mathbf{p}}, \quad (7)$$

where $\boldsymbol{\Lambda} = \boldsymbol{\Lambda}^\top > 0$ is a control gain, and the terms $\tilde{\mathbf{p}} \in \mathbb{R}^6$ and $\boldsymbol{\nu}_d \in \mathbb{R}^6$ are the pose tracking error and desired augmented velocity, respectively, which are defined in the following subsection for different choices of attitude parameterizations, along with the matrix $\mathbf{P} \in \mathbb{R}^{6 \times 6}$. The variable $\boldsymbol{\nu}_r$ is related to the virtual reference trajectory in [29], but is designed in a distinct manner to accommodate various attitude parameterizations, as outlined in Section III-B. Although (6) includes the desired trajectory, the presence of $\tilde{\mathbf{p}}$ introduces feedback within \mathbf{f}_d , which is why the term ‘‘feedforward-based control input’’ is used. The feedforward-based input in (6) can be alternatively written as

$$\mathbf{f}_d = \mathbf{W}\mathbf{a}, \quad (8)$$

where $\mathbf{a}^\top = [m_p \ I_{11} \ I_{22} \ I_{33} \ I_{12} \ I_{13} \ I_{23}]$, I_{ij} represent the six unique entries of \mathbf{I}_p , and $\mathbf{W} = \frac{\partial \mathbf{f}_d}{\partial \mathbf{a}}$. The term \mathbf{W} is a function of $\boldsymbol{\nu}_r$, $\dot{\boldsymbol{\nu}}_r$, and $\boldsymbol{\omega}^{pa}$, while \mathbf{a} is equivalent to the minimal parameter formulation developed in [29].

In practice, the entries of \mathbf{a} are not known exactly, so instead an estimate of \mathbf{a} is employed, which is denoted as $\hat{\mathbf{a}}$. The adaptive control input in (5) is defined as

$$\mathbf{f}_{ff} = \mathbf{W}\hat{\mathbf{a}}, \quad (9)$$

where $\hat{\mathbf{a}}$ evolves through the adaptive update law

$$\dot{\hat{\mathbf{a}}} = -\boldsymbol{\Upsilon}\mathbf{W}^\top\tilde{\boldsymbol{\nu}}_r, \quad (10)$$

and $\boldsymbol{\Upsilon} = \boldsymbol{\Upsilon}^\top > 0$ is a constant used to adjust the adaptation rate [27]. Subtracting (6) from (4), assuming the dynamics of the CDRP in (4) are dominated by those of its rigid-body payload, and substituting the expressions for the control inputs (5), and (9) yields the error dynamics

$$\mathbf{M}(\boldsymbol{\rho})\dot{\tilde{\boldsymbol{\nu}}}_r + \mathbf{D}(\boldsymbol{\rho}, \boldsymbol{\nu})\tilde{\boldsymbol{\nu}}_r = \mathbf{f} - \mathbf{f}_d = \mathbf{W}\tilde{\mathbf{a}} + \mathbf{f}_{fb}, \quad (11)$$

where $\tilde{\mathbf{a}} = \hat{\mathbf{a}} - \mathbf{a}$ and

$$\tilde{\boldsymbol{\nu}}_r = \boldsymbol{\nu} - \boldsymbol{\nu}_r = \boldsymbol{\nu} - (\boldsymbol{\nu}_d - \mathbf{P}\Lambda\tilde{\mathbf{p}}) = \tilde{\boldsymbol{\nu}} + \mathbf{P}\Lambda\tilde{\mathbf{p}}, \quad (12)$$

$\tilde{\boldsymbol{\nu}} = \boldsymbol{\nu} - \boldsymbol{\nu}_d$. Note that since \mathbf{a} is constant, $\dot{\hat{\mathbf{a}}} = \dot{\mathbf{a}}$.

B. Feedback Variable Formulation with Various Parameterizations of Payload Attitude

One of the main contributions of this paper is extending the control formulation of [27] to accommodate quaternion and $SO(3)$ attitude parameterizations. This extension relies on the derivation of a suitable filtered error system output for each parameterization that yields a passive input-output mapping and fits within the control formulation of [27].

The filtered error output is of the form

$$\mathbf{s} = \dot{\tilde{\mathbf{p}}} + \Lambda\tilde{\mathbf{p}}, \quad (13)$$

where $\Lambda = \Lambda^T > 0$ is a proportional-like control gain that is also featured in the definition of $\boldsymbol{\nu}_r$ in (7). In order to demonstrate a passive input-output mapping, closed-loop input-output stability, and convergence of the pose tracking error in Section III-C, it is required that $\tilde{\boldsymbol{\nu}}_r = \boldsymbol{\nu} - \boldsymbol{\nu}_r = \mathbf{P}\mathbf{s}$, where $\boldsymbol{\nu}_r$ is a function of $\boldsymbol{\nu}_d$, \mathbf{P} , and $\tilde{\mathbf{p}}$. The remainder of this subsection focuses on determining suitable choices of \mathbf{P} , $\tilde{\mathbf{p}}$, and $\boldsymbol{\nu}_d$ that ensures this property is satisfied for different choices of attitude parameterizations.

1) *Unconstrained Attitude Parameterizations:* Unconstrained attitude parameterizations, such as Euler-angle sequences, the rotation vector, and modified Rodrigues parameters (MRPs), are made up of 3 parameters that are free to evolve in time without any constraints, but suffer from singularities at one or more attitudes. For example, the 3-2-1 Euler-angle sequence described by the parameters $\mathbf{q}^{pa^T} = [\phi \ \theta \ \psi]$ has a kinematic singularity at $\theta = \pm\pi/2$, which results in the kinematic mapping matrix

$$\mathbf{S}(\mathbf{q}^{pa}) = \begin{bmatrix} 1 & 0 & -\sin\theta \\ 0 & \cos\phi & \sin\phi\cos\theta \\ 0 & -\sin\phi & \cos\phi\cos\theta \end{bmatrix}, \quad (14)$$

satisfying $\boldsymbol{\omega}^{pa} = \mathbf{S}(\mathbf{q}^{pa})\dot{\mathbf{q}}^{pa}$, to become singular [32].

Lemma 1: Consider an unconstrained attitude parameterization $\mathbf{q}^{pa} \in \mathbb{R}^3$. The definitions

$$\mathbf{P} = \begin{bmatrix} \mathbf{1} & \mathbf{0} \\ \mathbf{0} & \mathbf{S}(\mathbf{q}^{pa}) \end{bmatrix}, \quad (15)$$

$$\boldsymbol{\nu}_d = \mathbf{P} \begin{bmatrix} \dot{\mathbf{r}}_d \\ \dot{\mathbf{q}}^{da} \end{bmatrix}, \quad (16)$$

$$\tilde{\mathbf{p}} = \begin{bmatrix} \tilde{\mathbf{r}} \\ \mathbf{q}^{pa} - \mathbf{q}^{da} \end{bmatrix}, \quad (17)$$

where $\tilde{\mathbf{r}} = \mathbf{r} - \mathbf{r}_d$, ensure that $\tilde{\boldsymbol{\nu}}_r = \mathbf{P}\mathbf{s}$.

Proof: Substituting (17) into (13) and multiplying by (15) results in

$$\mathbf{P}\mathbf{s} = \mathbf{P} \left(\begin{bmatrix} \dot{\mathbf{r}} - \dot{\mathbf{r}}_d \\ \dot{\mathbf{q}}^{pa} - \dot{\mathbf{q}}^{da} \end{bmatrix} + \Lambda\tilde{\mathbf{p}} \right) = \mathbf{P} \begin{bmatrix} \dot{\mathbf{r}} \\ \dot{\mathbf{q}}^{pa} \end{bmatrix} - \mathbf{P} \begin{bmatrix} \dot{\mathbf{r}}_d \\ \dot{\mathbf{q}}^{da} \end{bmatrix} + \mathbf{P}\Lambda\tilde{\mathbf{p}}. \quad (18)$$

Multiplying out the first term in (18) and using the fact that $\boldsymbol{\omega}^{pa} = \mathbf{S}(\mathbf{q}^{pa})\dot{\mathbf{q}}^{pa}$ yields

$$\mathbf{P} \begin{bmatrix} \dot{\mathbf{r}} \\ \dot{\mathbf{q}}^{pa} \end{bmatrix} = \begin{bmatrix} \dot{\mathbf{r}} \\ \mathbf{S}(\mathbf{q}^{pa})\dot{\mathbf{q}}^{pa} \end{bmatrix} = \begin{bmatrix} \dot{\mathbf{r}} \\ \boldsymbol{\omega}^{pa} \end{bmatrix} = \boldsymbol{\nu}. \quad (19)$$

Substituting (19) into (18) and using (12) and (17) gives $\mathbf{P}\mathbf{s} = \tilde{\boldsymbol{\nu}} + \mathbf{P}\Lambda\tilde{\mathbf{p}} = \tilde{\boldsymbol{\nu}}_r$. ■

As in [27], the definition of $\boldsymbol{\nu}_d$ involves evaluating $\mathbf{S}(\mathbf{q}^{pa})$ with the payload attitude and not the desired attitude.

2) *Quaternion:* The quaternion $\mathbf{q}^{pa^T} = [\boldsymbol{\epsilon}^T \ \eta]$ is composed of the vector portion $\boldsymbol{\epsilon} \in \mathbb{R}^3$ and scalar part $\eta \in \mathbb{R}$, which satisfy the constraint $\mathbf{q}^{pa^T}\mathbf{q}^{pa} = \boldsymbol{\epsilon}^T\boldsymbol{\epsilon} + \eta^2 = 1$. The quaternion error is defined in [28], [32] as

$$\delta\mathbf{q} = \begin{bmatrix} \delta\boldsymbol{\epsilon} \\ \delta\eta \end{bmatrix} = \begin{bmatrix} \eta\mathbf{1} - \boldsymbol{\epsilon}^\times & \boldsymbol{\epsilon} \\ -\boldsymbol{\epsilon}^T & \eta \end{bmatrix} \begin{bmatrix} -\boldsymbol{\epsilon}_d \\ \eta_d \end{bmatrix}, \quad (20)$$

where $\mathbf{q}^{da^T} = [\boldsymbol{\epsilon}_d^T \ \eta_d]$ is the desired quaternion. The desired angular velocity is defined as a function of the rate of the desired quaternion as $\boldsymbol{\omega}^{da} = 2[\eta\mathbf{1} - \boldsymbol{\epsilon}^\times \ -\boldsymbol{\epsilon}] \dot{\mathbf{q}}^{da}$.

Lemma 2: Consider the quaternion attitude parameterization $\mathbf{q}^{pa} \in \mathbb{R}^4$. The definitions

$$\mathbf{P} = \begin{bmatrix} \mathbf{1} & \mathbf{0} \\ \mathbf{0} & 2(\delta\eta\mathbf{1} + \delta\boldsymbol{\epsilon}^\times)^{-1} \end{bmatrix}, \quad (21)$$

$$\boldsymbol{\nu}_d = \begin{bmatrix} \dot{\mathbf{r}}_d \\ \boldsymbol{\omega}^{da} + 2(\delta\eta\mathbf{1} + \delta\boldsymbol{\epsilon}^\times)^{-1}\boldsymbol{\omega}^{da^\times}\delta\boldsymbol{\epsilon} \end{bmatrix}, \quad (22)$$

$$\tilde{\mathbf{p}} = \begin{bmatrix} \tilde{\mathbf{r}} \\ \delta\boldsymbol{\epsilon} \end{bmatrix}, \quad (23)$$

ensure that $\tilde{\boldsymbol{\nu}}_r = \mathbf{P}\mathbf{s}$, where $\delta\boldsymbol{\epsilon}$ and $\delta\eta$ are defined in (20).

Proof: Substituting (23) into (13) and multiplying by (21) results in

$$\mathbf{P}\mathbf{s} = \mathbf{P} \left(\begin{bmatrix} \dot{\tilde{\mathbf{r}}} \\ \delta\dot{\boldsymbol{\epsilon}} \end{bmatrix} + \Lambda\tilde{\mathbf{p}} \right) = \begin{bmatrix} \dot{\tilde{\mathbf{r}}} \\ 2(\delta\eta\mathbf{1} + \delta\boldsymbol{\epsilon}^\times)^{-1}\delta\dot{\boldsymbol{\epsilon}} \end{bmatrix} + \mathbf{P}\Lambda\tilde{\mathbf{p}}. \quad (24)$$

The term $\delta\dot{\boldsymbol{\epsilon}}$ can be expanded using the property [32]

$$\delta\dot{\boldsymbol{\epsilon}} = -\boldsymbol{\omega}^{da^\times}\delta\boldsymbol{\epsilon} + \frac{1}{2}(\delta\eta\mathbf{1} + \delta\boldsymbol{\epsilon}^\times)(\boldsymbol{\omega}^{pa} - \boldsymbol{\omega}^{da}).$$

Substituting this into (24) and making use of (22) yields

$$\mathbf{P}\mathbf{s} = \begin{bmatrix} \dot{\tilde{\mathbf{r}}} \\ \boldsymbol{\omega}^{pa} - \boldsymbol{\omega}^{da} - 2(\delta\eta\mathbf{1} + \delta\boldsymbol{\epsilon}^\times)^{-1}\boldsymbol{\omega}^{da^\times}\delta\boldsymbol{\epsilon} \end{bmatrix} + \mathbf{P}\Lambda\tilde{\mathbf{p}} = \tilde{\boldsymbol{\nu}} + \mathbf{P}\Lambda\tilde{\mathbf{p}} = \tilde{\boldsymbol{\nu}}_r. \quad \blacksquare$$

The inverse of the matrix $(\delta\eta\mathbf{1} + \delta\boldsymbol{\epsilon}^\times)$ that is used to define \mathbf{P} exists provided $\delta\eta \neq 0$. This singularity is avoided as long as \mathcal{F}_p and \mathcal{F}_d are within a $\pm\pi/2$ rad rotation of each other, which is to be expected for overconstrained CDPRs.

3) *SO(3) (The Direction Cosine Matrix):* The DCM can be used directly with the antisymmetric projection operator to form an attitude error and satisfy the desired property.

Lemma 3: Consider an $SO(3)$ description of attitude with the DCM $\mathbf{C}_{pa} \in SO(3)$. The definitions

$$\mathbf{P} = \begin{bmatrix} \mathbf{1} & \mathbf{0} \\ \mathbf{0} & -2((\text{tr}(\mathbf{C}_{pd})\mathbf{1} - \mathbf{C}_{pd}))^{-1} \end{bmatrix}, \quad (25)$$

$$\boldsymbol{\nu}_d = \begin{bmatrix} \dot{\mathbf{r}}_d \\ \boldsymbol{\omega}^{da} \end{bmatrix}, \quad (26)$$

$$\tilde{\mathbf{p}} = \begin{bmatrix} \tilde{\mathbf{r}} \\ \mathcal{P}(\mathbf{C}_{pd})^\vee \end{bmatrix}, \quad (27)$$

ensure that $\tilde{\boldsymbol{\nu}}_r = \mathbf{P}\mathbf{s}$, where $\mathbf{C}_{pd} = \mathbf{C}_{pa}\mathbf{C}_{da}^\top$ and \mathbf{C}_{da} represents the desired payload attitude.

Proof: Substituting (27) into (13) and multiplying by (27) gives

$$\mathbf{P}\mathbf{s} = \mathbf{P} \left(\begin{bmatrix} \dot{\tilde{\mathbf{r}}} \\ \frac{d}{dt}(\mathcal{P}(\mathbf{C}_{pd})^\vee) \end{bmatrix} + \Lambda\tilde{\mathbf{p}} \right). \quad (28)$$

Poisson's equation, $\dot{\mathbf{C}}_{pd} = -\boldsymbol{\omega}^{pd \times} \mathbf{C}_{pd}$, and the identities in (1) and (2) are used to compute

$$\begin{aligned} \frac{d}{dt}(\mathcal{P}(\mathbf{C}_{pd})^\vee) &= -\frac{1}{2}(\tilde{\boldsymbol{\omega}}^\times \mathbf{C}_{pd} + \mathbf{C}_{pd}^\top \tilde{\boldsymbol{\omega}}^\times)^\vee \\ &= -\frac{1}{2} \left(((\text{tr}(\mathbf{C}_{pd})\mathbf{1} - \mathbf{C}_{pd}) \tilde{\boldsymbol{\omega}})^\times \right)^\vee \\ &= -\frac{1}{2}(\text{tr}(\mathbf{C}_{pd})\mathbf{1} - \mathbf{C}_{pd}) \tilde{\boldsymbol{\omega}}, \end{aligned} \quad (29)$$

where $\tilde{\boldsymbol{\omega}} = \boldsymbol{\omega}^{pd} = \boldsymbol{\omega}^{pa} - \boldsymbol{\omega}^{da}$. Substituting (29) into (28) and using (26) yields

$$\mathbf{P}\mathbf{s} = \begin{bmatrix} \dot{\tilde{\mathbf{r}}} \\ \tilde{\boldsymbol{\omega}} \end{bmatrix} + \mathbf{P}\Lambda\tilde{\mathbf{p}} = \tilde{\boldsymbol{\nu}} + \mathbf{P}\Lambda\tilde{\mathbf{p}} = \tilde{\boldsymbol{\nu}}_r. \quad \blacksquare$$

The inverse of $((\text{tr}(\mathbf{C}_{pd})\mathbf{1} - \mathbf{C}_{pd}))$ in the definition of \mathbf{P} exists as long as $\text{tr}(\mathbf{C}_{pd}) \neq 1$. Similar to the case of the quaternion, this singularity is avoided as long as \mathcal{F}_p and \mathcal{F}_d are within a $\pm\pi/2$ rad rotation of each other, which is large enough to account for the wrench-feasible workspaces of most over-constrained CDPRs.

It is worth noting that the term \mathbf{W} in the adaptive feedforward-based control input of (9) relies on the computation of $\dot{\boldsymbol{\nu}}_r = \dot{\boldsymbol{\nu}}_d - (\dot{\mathbf{P}}\Lambda\tilde{\mathbf{p}} + \mathbf{P}\Lambda\dot{\tilde{\mathbf{p}}})$, which requires an expression for $\dot{\mathbf{P}}$. For the case of unconstrained attitude parameterizations, such as a 3-2-1 Euler-angle sequence, this involves simply taking the time derivative of $\mathbf{S}(\mathbf{q}^{pa})$. For the quaternion, this computation is more involved, where $\dot{\mathbf{P}}$ is solved for using the matrix product rule $\frac{d}{dt}(\mathbf{A}^{-1}) = -\mathbf{A}^{-1}\dot{\mathbf{A}}\mathbf{A}^{-1}$ to obtain

$$\dot{\mathbf{P}} = \text{diag}\{\mathbf{0}, -2(\delta\eta\mathbf{1} + \delta\epsilon^\times)^{-1}(\delta\dot{\eta}\mathbf{1} + \delta\dot{\epsilon}^\times)(\delta\eta\mathbf{1} + \delta\epsilon^\times)^{-1}\},$$

where $\delta\dot{\eta}$ and $\delta\dot{\epsilon}$ are found by differentiating (20) with respect to time. A similar procedure is used to compute $\dot{\mathbf{P}}$ when using the $SO(3)$ description of attitude, where

$$\begin{aligned} \dot{\mathbf{P}} &= \text{diag}\{\mathbf{0}, -2\boldsymbol{\Gamma}(\text{tr}(\dot{\mathbf{C}}_{pd})\mathbf{1} - \dot{\mathbf{C}}_{pd})\boldsymbol{\Gamma}\} \\ &= \text{diag}\{\mathbf{0}, -2\boldsymbol{\Gamma}(-\text{tr}(\tilde{\boldsymbol{\omega}}^\times \mathbf{C}_{pd})\mathbf{1} + \tilde{\boldsymbol{\omega}}^\times \mathbf{C}_{pd})\boldsymbol{\Gamma}\}, \end{aligned}$$

$\boldsymbol{\Gamma} = (\text{tr}(\mathbf{C}_{pd})\mathbf{1} - \mathbf{C}_{pd})^{-1}$, and Poisson's equation is used to simplify the expression for $\dot{\mathbf{C}}_{pd}$.

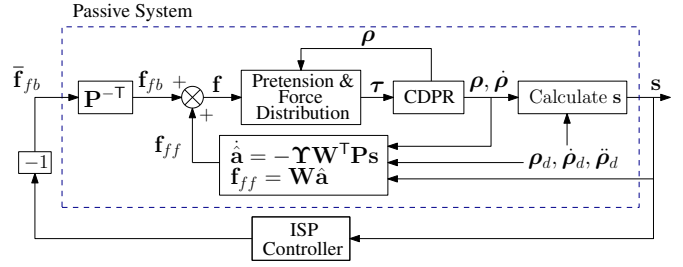


Fig. 2. Block diagram of a CDPR with an adaptive feedforward-based control input and pretension & force distribution satisfying $\mathbf{f} = \Pi^\top(\boldsymbol{\rho})\boldsymbol{\tau}$ which is proven to be passive in Theorem 1. The passive system is in negative feedback with an ISP controller.

C. Passivity and Closed-Loop Stability Analyses

Theorem 1: Consider a CDPR with error dynamics defined in (11) and the adaptive feedforward-based control input of (5) with the adaptive update law in (10). Assuming that the dynamics of the CDPR are dominated by its rigid-body payload, the input-output mapping $\mathbf{f}_{fb} \mapsto \mathbf{s}$ is passive, where $\mathbf{f}_{fb} = \mathbf{P}^\top \mathbf{f}_{fb}$.

Proof: Define the non-negative function

$$V_1 = \frac{1}{2}\tilde{\boldsymbol{\nu}}_r^\top \mathbf{M}\tilde{\boldsymbol{\nu}}_r + \frac{1}{2}\tilde{\mathbf{a}}^\top \boldsymbol{\Upsilon}^{-1}\tilde{\mathbf{a}}.$$

Taking the derivative of V_1 , substituting in the adaptive update law and (11) results in

$$\begin{aligned} \dot{V}_1 &= \tilde{\boldsymbol{\nu}}_r^\top \mathbf{M}\dot{\tilde{\boldsymbol{\nu}}_r} + \frac{1}{2}\tilde{\boldsymbol{\nu}}_r^\top \dot{\mathbf{M}}\tilde{\boldsymbol{\nu}}_r + \tilde{\mathbf{a}}^\top \boldsymbol{\Upsilon}^{-1}\dot{\tilde{\mathbf{a}}} \\ &= \tilde{\boldsymbol{\nu}}_r^\top (\mathbf{W}\tilde{\mathbf{a}} + \mathbf{f}_{fb}) + \frac{1}{2}\tilde{\boldsymbol{\nu}}_r^\top (\dot{\mathbf{M}} - 2\mathbf{D})\tilde{\boldsymbol{\nu}}_r - \tilde{\mathbf{a}}^\top \mathbf{W}^\top \tilde{\boldsymbol{\nu}}_r \\ &= \tilde{\boldsymbol{\nu}}_r^\top \mathbf{f}_{fb} = (\mathbf{P}\mathbf{s})^\top \mathbf{f}_{fb} = \mathbf{s}^\top \bar{\mathbf{f}}_{fb}. \end{aligned} \quad (30)$$

Integrating (30) from $t = 0$ to $t = T$, where $T \in \mathbb{R}_{\geq 0}$ gives

$$\int_0^T \mathbf{s}^\top \bar{\mathbf{f}}_{fb} dt = V_1(T) - V_1(0) \geq -V_1(0),$$

which proves the mapping $\bar{\mathbf{f}}_{fb} \mapsto \mathbf{s}$ is passive. \blacksquare

Corollary 1: The closed-loop system involving the CDPR with error dynamics defined in (11), the adaptive feedforward-based control input of (5), and an ISP negative feedback controller (or alternatively a linear time-invariant (LTI) strictly positive real (SPR) negative feedback controller) is input-output stable (i.e., $\mathbf{s} \in \mathcal{L}_2$).

Proof: Knowing that the input-output mapping $\bar{\mathbf{f}}_{fb} \mapsto \mathbf{s}$ is passive and an ISP controller is implemented in a negative feedback connection with this mapping (see Fig. 2), the passivity theorem guarantees that $\mathbf{s} \in \mathcal{L}_2$ [8, p. 358]. In the case of an SPR feedback controller, Theorem 8.10 in [35, p. 219] can be used to obtain the same result. \blacksquare

Corollary 1 guarantees closed-loop input-output stability with the use of any ISP or SPR feedback controller. This result does not rely on exact knowledge of the parameters of the CDPR's dynamics, and thus, robust closed-loop input-output stability is guaranteed. However, it is worth noting that robustness to pose estimation error is not guaranteed and falls beyond the scope of this work. Although there are a number of ISP controllers that can be used to ensure closed-loop input-output stability, an SPR controller with transfer matrix $\mathbf{G}_c(s) = \mathbf{C}_c(s\mathbf{1} - \mathbf{A}_c)^{-1}\mathbf{B}_c$ is considered in this paper. The

SPR property of $\mathbf{G}_c(s)$ ensures that there exist $\mathbf{P}_c = \mathbf{P}_c^\top > 0$ and $\mathbf{Q}_c = \mathbf{Q}_c^\top > 0$ such that [8, p. 93]

$$\begin{aligned}\mathbf{P}_c \mathbf{A}_c + \mathbf{A}_c^\top \mathbf{P}_c &= -\mathbf{Q}_c, \\ \mathbf{P}_c \mathbf{B}_c &= \mathbf{C}_c^\top.\end{aligned}$$

The feedback control input is then chosen as $\mathbf{f}_{fb} = -\mathbf{P}^{-\top} \mathbf{y}_c$, which results in $\dot{\mathbf{f}}_{fb} = \mathbf{P}^\top \mathbf{f}_{fb} = -\mathbf{P}^\top (\mathbf{P}^{-\top} \mathbf{y}_c) = -\mathbf{y}_c$, where $\mathbf{y}_c(s) = \mathbf{G}_c(s)\mathbf{s}(s)$.

Theorem 2: The control law in (5) and (9), where $\mathbf{f}_{fb} = -\mathbf{P}^{-\top} \mathbf{y}_c$ and \mathbf{y}_c is the output of an SPR controller with input \mathbf{s} , ensures asymptotic convergence of the pose tracking and rate tracking errors (i.e., $\tilde{\mathbf{p}} \rightarrow \mathbf{0}$ and $\tilde{\mathbf{v}} \rightarrow \mathbf{0}$ as $t \rightarrow \infty$), when applied to the CDRP with dynamics given by (4).

Proof: From Corollary 1, it is known that $\mathbf{s} \in \mathcal{L}_2$. Rearranging (13) yields $\dot{\tilde{\mathbf{p}}} = -\Lambda \tilde{\mathbf{p}} + \mathbf{s}$, which is an asymptotically stable LTI system whose input is in \mathcal{L}_2 . This results in $\tilde{\mathbf{p}} \in \mathcal{L}_2 \cap \mathcal{L}_\infty$, $\dot{\tilde{\mathbf{p}}} \in \mathcal{L}_2$, and $\tilde{\mathbf{p}} \rightarrow \mathbf{0}$ as $t \rightarrow \infty$ [8, p. 269]. To prove that $\tilde{\mathbf{v}} \rightarrow \mathbf{0}$ as $t \rightarrow \infty$, define the non-negative function

$$V_2 = V_1 + \mathbf{x}_c^\top \mathbf{P}_c \mathbf{x}_c,$$

where $\mathbf{P}_c = \mathbf{P}_c^\top > 0$. Making use of the SPR property of the feedback controller, the time derivative of V_2 is

$$\begin{aligned}\dot{V}_2 &= -\mathbf{s}^\top \mathbf{y}_c + \mathbf{x}_c^\top (\mathbf{P}_c \mathbf{A}_c + \mathbf{A}_c^\top \mathbf{P}_c) \mathbf{x}_c + \mathbf{x}_c^\top \mathbf{P}_c \mathbf{B}_c \mathbf{s} \\ &\leq -\mathbf{s}^\top \mathbf{y}_c - \mathbf{x}_c^\top \mathbf{Q}_c \mathbf{x}_c + \mathbf{x}_c^\top \mathbf{C}_c^\top \mathbf{s} \\ &\leq -\mathbf{s}^\top \mathbf{y}_c - \lambda_{\min}(\mathbf{Q}_c) \mathbf{x}_c^\top \mathbf{x}_c + \mathbf{y}_c^\top \mathbf{s} \\ &\leq -\lambda_{\min}(\mathbf{Q}_c) \mathbf{x}_c^\top \mathbf{x}_c \leq 0.\end{aligned}\quad (31)$$

Integrating (31) from $t = 0$ to $t = T$ results in $V_2(T) \leq V_2(0)$, which proves that $\{\tilde{\mathbf{v}}_r, \tilde{\mathbf{a}}, \mathbf{x}_c\} \in \mathcal{L}_\infty$. Through the relationship $\mathbf{s} = \mathbf{P}^{-1} \tilde{\mathbf{v}}_r$, where \mathbf{P}^{-1} is bounded, it is known that $\mathbf{s} \in \mathcal{L}_\infty$. This also results in $\dot{\tilde{\mathbf{p}}} \in \mathcal{L}_\infty$, since $\dot{\tilde{\mathbf{p}}} = -\Lambda \tilde{\mathbf{p}} + \mathbf{s}$. Assuming that $\nu_d \in \mathcal{L}_\infty$ and \mathbf{P} is bounded, $\tilde{\mathbf{p}} \in \mathcal{L}_\infty$ ensures that $\nu_r \in \mathcal{L}_\infty$ through (7). Taking the time derivative of (7) yields $\dot{\nu}_r = \dot{\nu}_d - (\dot{\mathbf{P}} \Lambda \tilde{\mathbf{p}} + \mathbf{P} \Lambda \dot{\tilde{\mathbf{p}}})$. Assuming that $\dot{\nu}_r \in \mathcal{L}_\infty$ and $\dot{\mathbf{P}}$ is bounded, $\{\tilde{\mathbf{p}}, \dot{\tilde{\mathbf{p}}}\} \in \mathcal{L}_\infty$ ensures $\dot{\nu}_r \in \mathcal{L}_\infty$. With $\{\nu_r, \dot{\nu}_r, \tilde{\mathbf{a}}, \mathbf{x}_c\} \in \mathcal{L}_\infty$, $\mathbf{f} - \mathbf{f}_d = \mathbf{W} \tilde{\mathbf{a}} - \mathbf{C}_c \mathbf{x}_c \in \mathcal{L}_\infty$. Through the error dynamics of (11), $\{\tilde{\mathbf{v}}_r, \mathbf{f} - \mathbf{f}_d\} \in \mathcal{L}_\infty$ results in $\dot{\tilde{\mathbf{v}}}_r \in \mathcal{L}_\infty$. Knowing that $\mathbf{s} \in \mathcal{L}_2$, the relationship $\tilde{\mathbf{v}}_r = \mathbf{P} \mathbf{s}$ leads to $\tilde{\mathbf{v}}_r \in \mathcal{L}_2$. Barbalat's lemma can be used to prove $\tilde{\mathbf{v}}_r \rightarrow \mathbf{0}$ as $t \rightarrow \infty$, since $\tilde{\mathbf{v}}_r \in \mathcal{L}_2$ and $\dot{\tilde{\mathbf{v}}}_r \in \mathcal{L}_\infty$ [8, p. 657]. It then follows that $\tilde{\mathbf{v}} \rightarrow \mathbf{0}$ as $t \rightarrow \infty$, since $\tilde{\mathbf{v}} = \tilde{\mathbf{v}}_r - \mathbf{P} \Lambda \tilde{\mathbf{p}}$ and both $\tilde{\mathbf{v}}_r \rightarrow \mathbf{0}$ and $\tilde{\mathbf{p}} \rightarrow \mathbf{0}$ as $t \rightarrow \infty$. ■

Theorem 2 demonstrates that the proposed control law ensures that $\tilde{\mathbf{r}} \rightarrow \mathbf{0}$ and $\tilde{\mathbf{p}} \rightarrow \mathbf{0}$ as $t \rightarrow \infty$. This results in the position of the CDRP's payload satisfying $\mathbf{r} \rightarrow \mathbf{r}_d$ as $t \rightarrow \infty$. The interpretation of $\tilde{\mathbf{p}} \rightarrow \mathbf{0}$ as $t \rightarrow \infty$ depends on the chosen attitude parameterization: $\mathbf{q}^{pa} \rightarrow \mathbf{q}^{da}$ for unconstrained attitude parameterizations, $\delta \epsilon \rightarrow \mathbf{0}$ (equivalent to $\mathbf{q}^{pa} \rightarrow \pm \mathbf{q}_d$) for the quaternion, and $\mathbf{C}_{pa} \rightarrow \mathbf{C}_{da}$ for $SO(3)$, all of which describe asymptotic convergence of the attitude of the CDRP's payload to the desired attitude. Note that as in [7], [27], [29], there is no guarantee that $\hat{\mathbf{a}} \rightarrow \mathbf{a}$ as $t \rightarrow \infty$, as $\hat{\mathbf{a}}$ evolves in a manner that only guarantees asymptotic tracking of the desired payload pose.

TABLE I

CDRP PARAMETERS USED IN THE NUMERICAL SIMULATION.

Parameter	Value
Payload mass (kg)	$m_p = 6.75$
Payload inertia (g·m ²)	$\mathbf{I}_p = \text{diag}\{15.8, 5.2, 14.7\}$
Cable density (g/m)	$\rho = 4.6$
Cable elasticity (N/m ²)	$E = 127 \times 10^9$
Cable Radius (mm)	$r_c = 1$
Winch radius (m)	$r_i = 0.0254, i = 1, \dots, 8$
Winch inertia (g·m ²)	$J_i = 0.025, i = 1, \dots, 8$

TABLE II

CABLE ATTACHMENT POINTS IN THE NUMERICAL SIMULATION.

Cable	Winch Position Rel. to Origin in \mathcal{F}_a (cm)	Payload Attachment Rel. to Payload CoM in \mathcal{F}_p (cm)
1	[71 38 93]	[3 7.5 -3.75]
2	[-71 38 93]	[-3 7.5 -3.75]
3	[-71 -38 93]	[-3 -7.5 -3.75]
4	[71 -38 93]	[3 -7.5 -3.75]
5	[-71 -38 0]	[-1.5 -7.5 3.75]
6	[71 38 0]	[1.5 7.5 3.75]
7	[-71 38 0]	[-1.5 7.5 3.75]
8	[71 -38 0]	[1.5 -7.5 3.75]

IV. CDRP NUMERICAL EXAMPLE

Consider a 6 DOF CDRP with $m = 8$ cables and a rigid-body payload, as shown in Fig. 1, with numerical provided in Table I. The locations of the 8 stationary winches and the attachment points of the cables on the rigid-body payload are given in Table II. A crossed-cable configuration similar to the IPAnema 2 setup described in [1, p. 319] is used, which results in a relatively large wrench-feasible translational and rotational workspace while avoiding cable collisions.

The numerical simulation is fashioned from the Lagrangian-based dynamic model developed in [15] for flexible cables whose mass and stiffness properties vary with the length of the cable, and is extended to accommodate a 6 DOF, 8-cable CDRP. A first set of simulations is performed with cables modeled as rigid straight lines, where the elastic coordinates of the model from [15] are constrained to be zero (i.e., no elastic deformation can occur). The second set of simulations models elastic deformation of the cables in the axial and two transverse directions with the Rayleigh-Ritz method in [15]. Both numerical models include cable mass and allow the cables to transmit forces only when under tension. An aramid cable with properties listed in Table I is used. In the case with flexible cables, the pose of the payload used by the controller is computed through forward kinematics [33] using only the rigid rotation of the winches in order to simulate a realistic implementation scenario and demonstrate robustness to imperfect knowledge of the payload pose. All pose tracking errors in the result plots are of the actual payload pose, computed using the deformed cables.

The desired payload position trajectory is $\mathbf{r}_d^\top = 0.1[\cos(0.6\pi t) \sin(0.6\pi t) \cos(0.6\pi t) + 4.65]$ m and the desired payload attitude trajectory is $\mathbf{q}^{da^\top} = 20[\cos(0.4\pi t - \pi/2) \cos(0.4\pi t - \pi/4) \cos(0.4\pi t)]$ deg,

described in terms of a 3-2-1 Euler-angle sequence. Note that while an Euler-angle sequence is used here to define the desired attitude trajectory, any attitude parameterization can be used for this purpose and converted to the attitude parameterization chosen for the controller.

Numerical simulations are performed with the proposed adaptive control law using various payload attitude parameterizations, including a 3-2-1 Euler angle sequence, $SO(3)$ (the DCM), the quaternion, the rotation vector, and MRF. As a comparison, two simplifications of the proposed controller with a 3-2-1 Euler angle sequence are also tested in simulation, where small Euler angles are assumed (i.e., $\boldsymbol{\omega}^{pa} \approx \dot{\mathbf{q}}^{pa}$) in either the feedback controller and the adaptive feedforward-based controller (denoted as Simplified Euler) or only the feedback controller (denoted as Simplified FB Euler). These simplifications are similar to the linear control design and analysis performed in [23].

The negative feedback controller is implemented as $\mathbf{f}_{fb} = -\mathbf{P}^{-T}\mathbf{y}_c$, where \mathbf{y}_c is the output of an SPR controller with feedthrough and input \mathbf{s} . A variety of methods can be used to design an SPR controller (e.g., see [36]) and in this work a simple first-order low-pass filter

$$\mathbf{y}_c(s) = \mathbf{K}_d \text{diag} \left\{ \frac{\omega_c}{s + \omega_c}, \dots, \frac{\omega_c}{s + \omega_c} \right\} \mathbf{s}(s),$$

where $\mathbf{K}_d = \mathbf{K}_d^T > 0$ is the derivative gain, $\omega_c = 2\pi$ rad/s is the chosen cut-off frequency. The inertia entries of $\hat{\mathbf{a}}$ are all initially set to zero, while the payload mass is assumed to be approximately known and therefore \hat{m}_p is initialized within 20% of the true payload mass. The control parameters used for the rigid cable simulation are $\boldsymbol{\Lambda} = 10 \cdot \mathbf{1}$, $\boldsymbol{\Upsilon} = 5 \cdot \mathbf{1}$, $\mathbf{K}_d = \text{diag}\{\mathbf{K}_{d,v}, \mathbf{K}_{d,\omega}\}$, $\mathbf{K}_{d,v} = 125 \cdot \mathbf{1}$, and $\mathbf{K}_{d,\omega} = 16\frac{2}{3} \cdot \mathbf{1}$. For the quaternion-based controller, \mathbf{K}_d is doubled to ensure the control gain is the same for small angles across all attitude parameterizations and a fair performance comparison can be made (i.e., $\delta\epsilon \approx \frac{1}{2}\mathbf{q}^{pa}$, where \mathbf{q}^{pa} is an unconstrained attitude parameterization). The control gains when simulating the CDPR with flexible cables are reduced to increase robustness to the unmodeled dynamics. Specifically, the terms \mathbf{K}_d and $\boldsymbol{\Lambda}$ are reduced by a factor of 5 and 2, respectively. This is a common strategy used when controlling the motion of a CDPR with flexible cables [13].

The control wrench, \mathbf{f} , is distributed to the winch torques, $\boldsymbol{\tau}$, using the improved closed-form solution from [1] as

$$\boldsymbol{\tau} = \boldsymbol{\tau}_{pt} + \mathbf{U}^T(\boldsymbol{\theta}) \left(\mathbf{f} - \boldsymbol{\Pi}^T(\boldsymbol{\rho})\boldsymbol{\tau}_{pt} \right), \quad (32)$$

where $\boldsymbol{\tau}_{pt} = \text{diag}\{r_1, \dots, r_8\}\mathbf{t}_{pt}$ is a pretension torque, r_i is the radius of the i^{th} winch, $\mathbf{t}_{pt} \in \mathbb{R}^8$ contains the desired pretension in the 8 cables, and $\mathbf{U}(\boldsymbol{\theta})$ is a pseudo-inverse of $\boldsymbol{\Pi}(\boldsymbol{\rho})$. A pretension value of 59 N is used for each cable, with the goal of ensuring that the cable tensions are greater than 7.9 N and less than 3937 N. If at a particular instance in time, a cable tension exceeds the allowed range, the algorithm sets the cable tension to the limiting value and recomputes (32) with the row associated with that particular cable removed.

Simulation results are presented in Figs. 3 through 8, including detailed results for the case of flexible cables and

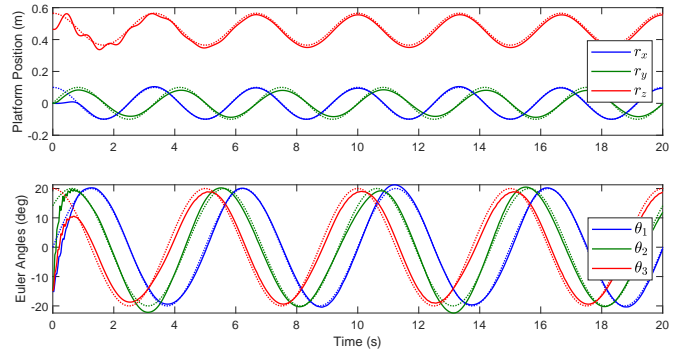


Fig. 3. Payload pose trajectory versus time with the $SO(3)$ -based controller simulated with flexible cables: actual pose (solid) and desired pose (dashed). The payload attitude is expressed in terms of a 3-2-1 Euler-angle sequence only for visualization purposes.

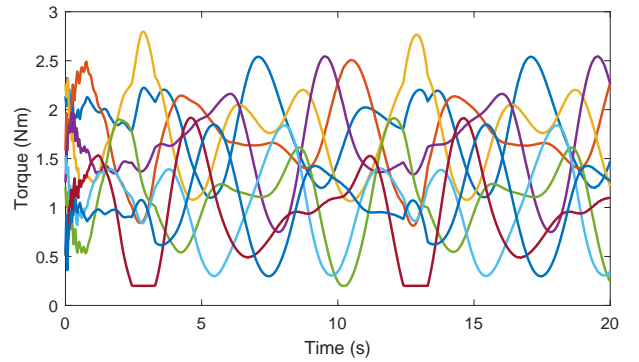


Fig. 4. Winch torques versus time for the simulation with the $SO(3)$ -based controller and flexible cables.

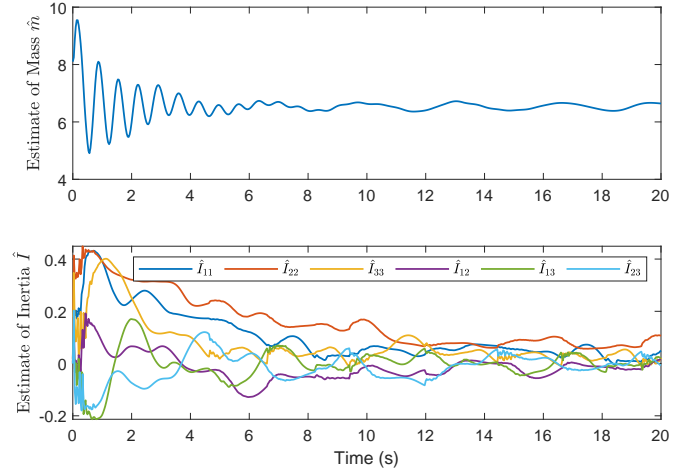


Fig. 5. Estimated parameters $\hat{\mathbf{a}}$ versus time for the simulation with the $SO(3)$ -based controller and flexible cables. The two subplots are the mass parameter (denoted \hat{m}) and inertial parameters (denoted \hat{I}_{ij}).

the $SO(3)$ -based controller in Figs. 3, 4, and 5. Specifically, Fig. 3 features the desired payload pose and the closed-loop response of the payload pose, where $\mathbf{r}^T(0) = [0 \ 0 \ 0.465] \text{ m}$ and the initial payload attitude is associated with a 3-2-1 Euler angle sequence with all angles equal to -15 deg. The CDPR's winch torques as a function of time are included in Fig. 4 to demonstrate that positive cable

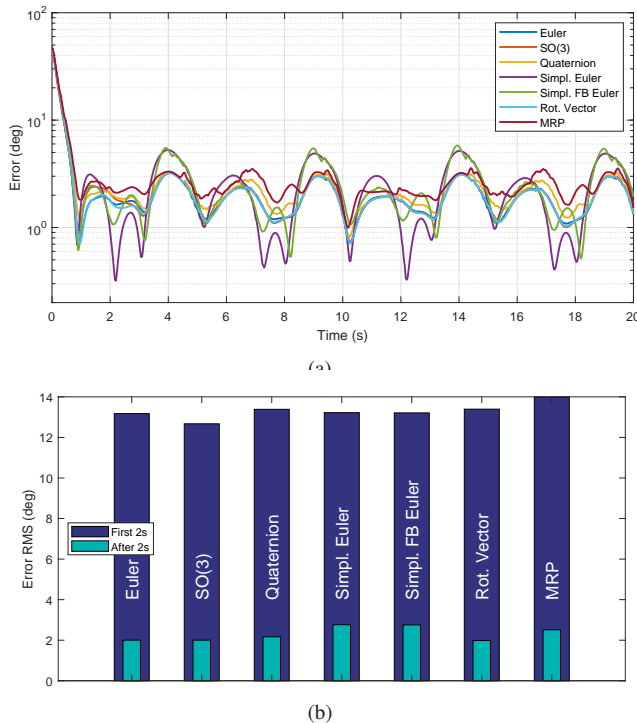


Fig. 6. (a) Attitude tracking error versus time and (b) RMS attitude tracking error with controllers based on different attitude parameterizations for the case of flexible cables. The error is the angle portion of an axis-angle parameterization of the attitude tracking error.

tensions are maintained. Fig. 5 includes the estimated system parameters \hat{a} as a function of time.

The complete set of simulated controllers is compared by computing the axis-angle parameters associated with the attitude tracking error. The resulting error angle is plotted versus time in Fig. 6(a). To further quantify the differences in attitude tracking errors, the root mean square (RMS) value of the error angle is shown in Fig. 6(b) for the seven controllers and is separated into the RMS error of the transient response during the first 2 seconds of the simulation and the steady-state response after the first 2 seconds of the simulation. The comparisons in Fig. 6 demonstrate that the Simplified Euler and Simplified FB Euler controllers lead to the least consistent tracking errors, particularly in their steady-state responses. This is also evident in Fig. 6(b), where the RMS attitude tracking errors are largest for these controllers after the first 2 seconds. For a visual comparison, the pose tracking errors versus time are included for the Simplified Euler, Euler, and $SO(3)$ -based controllers with rigid cables in Fig. 7 and flexible cables in Fig. 8. Quick convergence of the tracking error is seen with rigid cables in Fig. 7 and reasonably small tracking error is present with the flexible cables in Fig. 8, which demonstrates the robustness of the proposed controller. The Simplified Euler controller features larger oscillations in tracking errors compared to both the Euler-angle and $SO(3)$ -based controllers.

V. CONCLUSION

This paper presented an adaptive passivity-based CDPR pose tracking controller for various attitude parameterizations. The benefit of performing CDPR pose tracking with carefully defined attitude errors was demonstrated, where a linearized Euler-angle parameterization was shown to yield inferior tracking results. Closed-loop asymptotic convergence of the pose tracking error was proven and shown to be robust to parameter uncertainty through nonlinear stability analysis and also in simulation with a CDPR that featured unmodeled and uncertain flexible cable dynamics.

Future work will focus on experimental implementation of the proposed control law on multiple trajectories and explicit consideration of flexible cables in the controller formulation and stability analysis.

REFERENCES

- [1] A. Pott, *Cable-Driven Parallel Robots*. Cham, Switzerland: Springer International, 2018.
- [2] J. Lamaury, M. Gouttefarde, A. Chemori, and P.-E. Hervé, “Dual-space adaptive control of redundantly actuated cable-driven parallel robots,” in *IEEE Int. C. Int. Robot.*, 2013, pp. 4879–4886.
- [3] R. Babaghasabha, M. A. Khosravi, and H. D. Taghirad, “Adaptive robust control of fully constrained cable robots: singular perturbation approach,” *Nonlinear Dynam.*, vol. 85, no. 1, pp. 607–620, 2016.
- [4] H. Ji, W. Shang, and S. Cong, “Adaptive synchronization control of cable-driven parallel robots with uncertain kinematics and dynamics,” *IEEE T. Ind. Electron.*, vol. 68, no. 9, pp. 8444–8454, 2020.
- [5] W. Shang, F. Xie, B. Zhang, S. Cong, and Z. Li, “Adaptive cross-coupled control of cable-driven parallel robots with model uncertainties,” *IEEE Robot. Autom. Lett.*, vol. 5, no. 3, pp. 4110–4117, 2020.
- [6] M. R. J. Harandi, S. Khalilpour, H. D. Taghirad, and J. G. Romero, “Adaptive control of parallel robots with uncertain kinematics and dynamics,” *Mechanical Syst. Signal Pr.*, vol. 157, p. 107693, 2021.
- [7] R. Ortega and M. W. Spong, “Adaptive motion control of rigid robots: A tutorial,” *Automatica*, vol. 25, no. 6, pp. 877–888, 1989.
- [8] B. Brogliato, R. Lozano, B. Maschke, and O. Egeland, *Dissipative Systems Analysis and Control: Theory and Applications*, 3rd ed. Cham, Switzerland: Springer International, 2020.
- [9] T. Shibata and T. Murakami, “Null space motion control by PID control considering passivity in redundant manipulator,” *IEEE T. Ind. Inform.*, vol. 4, no. 4, pp. 261–270, 2008.
- [10] H. Abdellatif, B. Heimann, and J. Kotlarski, “Passivity-based observer/controller design with desired dynamics compensation for 6 DOFs parallel manipulators,” in *IEEE Int. C. Int. Robot.*, 2008, pp. 2392–2397.
- [11] A. Hayes and R. J. Caverly, “Passivity-based control allocation of a redundantly-actuated parallel robotic manipulator with a point-mass payload,” in *Amer. Contr. Conf.*, 2020, pp. 2432–2437.
- [12] M. Zarebidoki, A. Lotfavar, and H. R. Fahham, “Effectiveness of adaptive passivity-based trajectory tracking control of a cable-suspended robot,” in *Int. Conf. Trends Mech. Indust. Eng.*, 2011, pp. 180–184.
- [13] R. J. Caverly, J. R. Forbes, and D. Mohammadshahi, “Dynamic modeling and passivity-based control of a single degree of freedom cable-actuated system,” *IEEE T. Contr. Syst. T.*, vol. 23, no. 3, pp. 898–909, 2015.
- [14] R. J. Caverly and J. R. Forbes, “Flexible cable-driven parallel manipulator control: Maintaining positive cable tensions,” *IEEE T. Contr. Syst. T.*, vol. 26, no. 5, pp. 1874–1883, 2018.
- [15] H. A. Godbole, R. J. Caverly, and J. R. Forbes, “Dynamic modeling and adaptive control of a single degree-of-freedom flexible cable-driven parallel robot,” *J. Dyn. Sys., Meas., Control*, vol. 141, no. 10, p. 101002, 2019.
- [16] S. Khalilpour, R. Khorrambakht, H. Damirchi, H. Taghirad, and P. Cardou, “Tip-trajectory tracking control of a deployable cable-driven robot via output redefinition,” *Multibody Syst. Dyn.*, vol. 52, no. 1, pp. 31–58, 2021.
- [17] S. K. Cheah and R. J. Caverly, “Passivity-based pose regulation and Jacobian-based force distribution of a cable-driven parallel robot,” in *Amer. Contr. Conf.*, 2021, pp. 124–129.

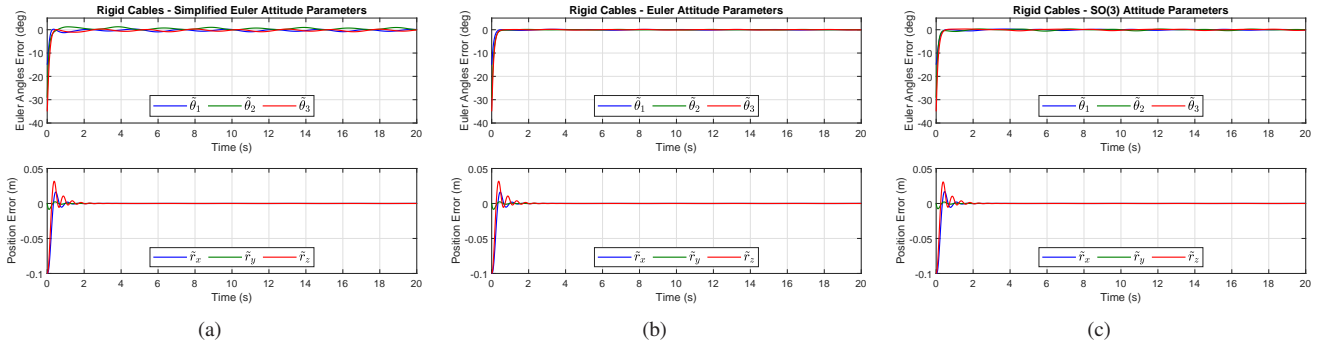


Fig. 7. Payload pose tracking errors in the rigid-cable simulations with (a) the simplified Euler-angle-based controller, (b) the correctly-implemented Euler-angle-based controller, and (c) the $SO(3)$ -based controller. For visualization purposes, the attitude errors are plotted using a 3-2-1 Euler-angle sequence (denoted θ_1 , θ_2 , and θ_3). The position errors in the three axes of \mathcal{F}_a are denoted as \tilde{r}_x , \tilde{r}_y , and \tilde{r}_z .

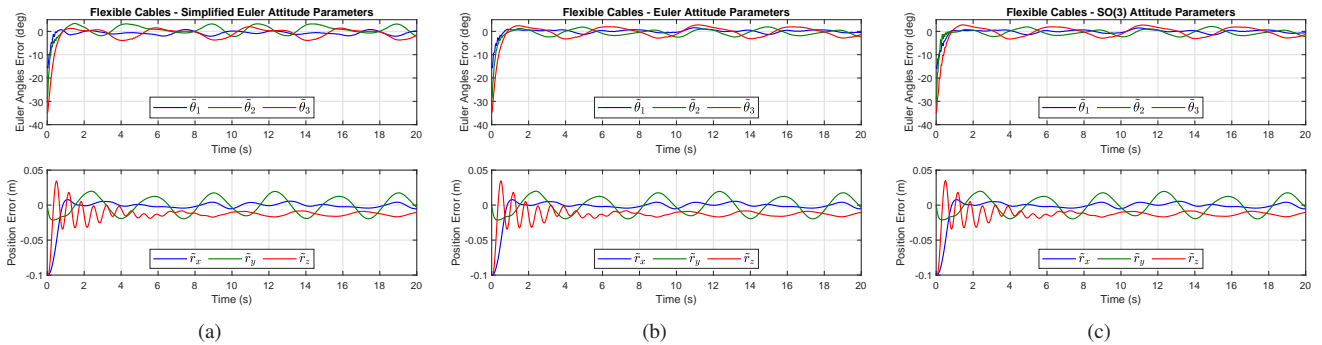


Fig. 8. Payload pose tracking errors in the flexible-cable simulations with (a) the simplified Euler-angle-based controller, (b) the correctly-implemented Euler-angle-based controller, and (c) the $SO(3)$ -based controller. For visualization purposes, the attitude errors are plotted using a 3-2-1 Euler-angle sequence (θ_1 , θ_2 , and θ_3). The position errors in the three axes of \mathcal{F}_a are denoted as \tilde{r}_x , \tilde{r}_y , and \tilde{r}_z .

- [18] M. H. Korayem, M. Yousefzadeh, and B. Beyranvand, "Dynamics and control of a 6-dof cable-driven parallel robot with visco-elastic cables in presence of measurement noise," *J. Intell. Robot. Syst.*, vol. 88, no. 1, pp. 73–95, 2017.
- [19] T. Bruckmann, L. Mikelsons, T. Brandt, M. Hiller, and D. Schramm, "Wire robots part II: Dynamics, control & application," in *Parallel Manipulators, New Developments*. Vienna, Austria: I-Tech Education and Publishing, 2008, ch. 7, pp. 133–152.
- [20] R. Chellal, L. Cuvillon, and E. Laroche, "Model identification and vision-based \mathcal{H}_∞ position control of 6-DoF cable-driven parallel robots," *Int. J. Control*, vol. 90, no. 4, pp. 684–701, 2017.
- [21] C. Schenk, C. Masone, A. Pott, and H. H. Bühlhoff, "Application of a differentiator-based adaptive super-twisting controller for a redundant cable-driven parallel robot," in *Int. Conf. Cable-Driven Parallel Robots*. Cham, Switzerland: Springer International, 2018, vol. 53, pp. 254–267.
- [22] J. Begey, L. Cuvillon, M. Lesellier, M. Gouttefarde, and J. Gangloff, "Dynamic control of parallel robots driven by flexible cables and actuated by position-controlled winches," *IEEE T. Robot.*, vol. 35, no. 1, pp. 286–293, 2019.
- [23] J. C. Santos, A. Chemori, and M. Gouttefarde, "Redundancy resolution integrated model predictive control of CDRPs: Concept, implementation and experiments," in *IEEE Int. Conf. Robot. Autom.*, 2020, pp. 3889–3895.
- [24] Z. Zake, F. Chaumette, N. Pedemonte, and S. Caro, "Vision-based control and stability analysis of a cable-driven parallel robot," *IEEE Rob. Autom. Lett.*, vol. 4, no. 2, pp. 1029–1036, 2019.
- [25] V. L. Nguyen and R. J. Caverly, "Cable-driven parallel robot pose estimation using extended Kalman filtering with inertial payload measurements," *IEEE Robot. Autom. Lett.*, vol. 6, no. 2, pp. 3615–3622, 2021.
- [26] Z. Zake, F. Chaumette, N. Pedemonte, and S. Caro, "Moving-platform pose estimation for cable-driven parallel robots," in *IEEE Int. C. Int. Robot.*, 2021, pp. 8036–8043.
- [27] C. J. Damaren, "Adaptive control of flexible manipulators carrying large uncertain payloads," *J. Rob. Syst.*, vol. 13, no. 4, pp. 219–228, 1996.
- [28] O. Egeland and J.-M. Godhavn, "Passivity-based adaptive attitude control of a rigid spacecraft," *IEEE T. Automat. Contr.*, vol. 39, no. 4, pp. 842–846, 1994.
- [29] J.-J. E. Slotine and W. Li, "On the adaptive control of robot manipulators," *Int. J. Robot. Res.*, vol. 6, no. 3, pp. 49–59, 1987.
- [30] J. R. Forbes, "Passivity-based attitude control on the special orthogonal group of rigid-body rotations," *J. Guid. Control Dynam.*, vol. 36, no. 6, pp. 1596–1605, 2013.
- [31] T.-H. Wu and T. Lee, "Angular velocity observer for attitude tracking on $SO(3)$ with the separation property," *Int. J. Control Autom.*, vol. 14, no. 5, pp. 1289–1298, 2016.
- [32] F. L. Markley and J. L. Crassidis, *Fundamentals of Spacecraft Attitude Determination and Control*. New York, NY: Springer, 2014.
- [33] V. L. Nguyen and R. J. Caverly, "CDPR forward kinematics with error covariance bounds for unconstrained end-effector attitude parameterizations," in *Int. Conf. Cable-Driven Parallel Robots*. Cham, Switzerland: Springer International, 2021, pp. 37–49.
- [34] M. A. Khosravi and H. D. Taghirad, "Dynamic modeling and control of parallel robots with elastic cables: Singular perturbation approach," *IEEE T. Robot.*, vol. 30, no. 3, pp. 694–704, 2014.
- [35] H. Marquez, *Nonlinear Control Systems*. Hoboken, NJ: Wiley, 2003.
- [36] R. J. Benhabib, R. P. Iwens, and R. L. Jackson, "Stability of large space structure control systems using positivity concepts," *J. Guid. Control*, vol. 4, no. 5, pp. 487–494, Sept.–Oct. 1981.